ISSN 1674-1056
http://cpb.iphy.ac.cn
http://iopscience.iop.org/cpb
中国物理 B
Chinese Physics
中国物理 Chinese Physics B

# Electron capture in collisions of $Li^{3+}$ ions with ground and excited states of Li atoms

M X Ma(马茗萱)[1,2,3], B H Kou(寇博珩)[4], L Liu(刘玲)[3], Y Wu(吴勇)[3], J G Wang(王建国)[3]

**Citation:**Chin. Phys. B . 2020, 29(1): 013401 . **doi:** 10.1088/1674-1056/ab577f
Journal homepage: http://cpb.iphy.ac.cn; http://iopscience.iop.org/cpb

**What follows is a list of articles you may be interested in**

---

## Non-adiabatic quantum dynamical studies of Na(3p)+HD($v$=1, $j$=0)→NaH/NaD+D/H reaction

Yue-Pei Wen(温月佩), Bayaer Buren(布仁巴雅尔), Mao-Du Chen(陈茂笃)
Chin. Phys. B . 2019, 28(6): 063401 . **doi:** 10.1088/1674-1056/28/6/063401

## Polarization and exchange effects in elastic scattering of electron with atoms and ions

Zhang-Jin Chen(陈长进), Dan-Dan Cui(崔丹丹)
Chin. Phys. B . 2018, 27(5): 053403 . **doi:** 10.1088/1674-1056/27/5/053403

## Electron-impact single ionizaiton for $W^{4+}$ and $W^{5+}$

Denghong Zhang(张登红), Luyou Xie(颉录有), Jun Jiang(蒋军), Zhongwen Wu(武中文), Chenzhong Dong(董晨钟), Yinglong Shi(师应龙), Yizhi Qu(屈一至)
Chin. Phys. B . 2018, 27(5): 053402 . **doi:** 10.1088/1674-1056/27/5/053402

## Differential cross sections of positron—hydrogen collisions

Rong-Mei Yu(于荣梅), Chun-Ying Pu(濮春英), Xiao-Yu Huang(黄晓玉), Fu-Rong Yin(殷复荣), Xu-Yan Liu(刘旭焱), Li-Guang Jiao(焦利光), Ya-Jun Zhou(周雅君)
Chin. Phys. B . 2016, 25(7): 073401 . **doi:** 10.1088/1674-1056/25/7/073401

## Influence of electron correlations on double-capture process in proton helium collisions

Hoda Ghavaminia, Ebrahim Ghanbari-Adivi
Chin. Phys. B . 2015, 24(7): 073401 . **doi:** 10.1088/1674-1056/24/7/073401

---

# Electron capture in collisions of $Li^{3+}$ ions with ground and excited states of Li atoms*

M X Ma(马茗萱)[1,2,3], B H Kou(寇博珩)[4], L Liu(刘玲)[3,†], Y Wu(吴勇)[3], and J G Wang(王建国)[3]

[1] *Institute of Modern Physics, Fudan University, Shanghai* 200433, *China*
[2] *Key Laboratory of Nuclear Physics and Ion-beam Application (MOE), Fudan University, Shanghai* 200433, *China*
[3] *Institute of Applied Physics and Computational Mathematics, Beijing* 100088, *China*
[4] *Kents Hill School, 12th Grade, Maine* 04349, *USA*

(Received 10 September 2019; revised manuscript received 4 November 2019; accepted manuscript online 14 November 2019)

The electron capture processes in collisions of $Li^{3+}$ ion with $Li(1s^22s)$ and $Li(1s^22p_{0,1})$ are investigated by using the two-center atomic orbital close-coupling method in the energy range from 0.1 keV/u to 300 keV/u. The interaction of the active electrons with the target ion is represented by a model potential. The present results for the $Li^{3+}$–$Li(1s^22s)$ system are compared with the available theoretical data and general agreement is obtained for the high collision energies. It is also found that the total and partial electron capture cross sections are sensitive to the initial charge cloud alignment in the low energy region.

**Keywords:** two-center atomic orbital closed coupling, electron capture, cross section

**PACS:** 34.70.+e, 52.20.Hv **DOI:** 10.1088/1674-1056/ab577f

## 1. Introduction

In the last several decades, considerable attention has been paid to the charge transfer processes in ion–atom collisions as these are the fundamental processes in many fields, such as astrophysics, laboratory plasmas, and controlled-thermonuclear fusion.[1–3] For instance, the neutral lithium beam has been injected into tokamaks to provide valuable diagnostic information of plasma parameters by analyzing the line-radiation following collisions of Li atoms with other particles.[4–6] Therefore, the study of collision dynamics involving Li is very important. However, the collision processes of $Li^{3+}$ with excited Li atom have received very limited attention. In the present work, we will focus on the charge transfer process in the collisions of $Li^{3+}$ with the ground and excited states of Li atoms

$$Li^{3+} + Li\left(1s^22s\right) \rightarrow Li^{2+} + Li^{+}, \quad (1)$$

$$Li^{3+} + Li\left(1s^22p_0\right) \rightarrow Li^{2+} + Li^{+}, \quad (2)$$

$$Li^{3+} + Li\left(1s^22p_1\right) \rightarrow Li^{2+} + Li^{+}, \quad (3)$$

in the energy range from 0.01 keV/u to 300 keV/u by employing the two-center atomic orbital close-coupling (TC-AOCC) method, where 0 and 1 in the subscript represent the magnetic quantum number of the p state.

To the best of our knowledge, no experimental data for the charge transfer processes (1)–(3) have been reported so far. On the theoretical side, Opradocle *et al.*[7] have finished the calculations of the total charge exchange cross section for process (1) by using the one-electron approximation method in the impact energy range $2.25 \times 10^{-4}$–1 keV/u. The semiclassical impact-parameter method based on a 15-state molecular-orbital expansion has been used by Kuma to calculate the total charge exchange cross sections for $Li^{3+}$–$Li(1s^22s)$ collisions.[8] Schweinzer *et al.*[9] used the atomic-orbital close-coupling method to study the electron capture and target excitation processes in collisions of $Li^{3+}$–$Li(1s^22s)$ at the low and intermediate energies. The total electron capture cross section was given for the energy range 0.5–5 keV/u. The classical trajectory Monte Carlo (CTMC) method was also employed to calculate the total and *n*-partial charge transfer cross sections by Otranto *et al.*[10] in the energy region 0.01–100 keV/u. However, the *nl*-state selective charge transfer cross sections for the $Li^{3+}$–$Li(1s^22s)$ system and the collisions involving excited Li atoms were not reported until now. In this work, we will present the total and state-selective cross sections for the collisions between $Li^{3+}$ and $Li(1s^22s)/Li(1s^22p_{0,1})$ in the energy range 0.1–300 keV/u.

The paper is organized as follows. In Section 2, we briefly describe the TC-AOCC method used in the present cross section calculations and give the model potential. In Section 3, we present the calculated results and discussion for the total and state-selective electron-capture cross sections. In Section 4, we give our conclusions. Atomic units will be used throughout this paper, unless otherwise explicitly indicated.

*Project supported by the National Key Research and Development Program of China (Grant No. 2017YFA0402300), the National Natural Science Foundation of China (Grant No. 11774037), International Atomic Energy Agency, China (Grant No. 23196/R0), and the Science Challenge Project of China (Grant No. TZ2016001).

†Corresponding author. E-mail: liu_ling@iapcm.ac.cn

© 2020 Chinese Physical Society and IOP Publishing Ltd 

## 2. Theoretical method

### 2.1. Two-center atomic orbital close-coupling method

The two-center atomic orbital close-coupling method is a semi-classical method for describing the collisions between ions and atoms (ions) in the intermediate energy region. The approximation of straight-line trajectories is used for the nuclear motion, and the details of this method can be found in Ref. [11]. Here only a short introduction is given.

The total wave function $\Psi$ of the collision system can be written in the form

$$\Psi = \sum_{j=1}^{N} A_j \Phi_j + \sum_{n=N+1}^{N+M} B_n \chi_n, \tag{4}$$

where the functions $\Phi_j$ and $\chi_n$ are atomic orbitals centered on the target and the projectile ion, respectively. The atomic orbitals can be determined by Slater basis in the form

$$\Phi = \sum_k C_{nk} N_l(\zeta_k)\, \mathrm{e}^{-\zeta_k r} r^J Y_{lm}(r), \tag{5}$$

$$\zeta_k = \alpha \beta^k, \quad k = 1, 2, \ldots, N, \tag{6}$$

where $C_{nk}$ is the expansion factor, $Y_{lm}(r)$ is the spherical harmonic function, $\alpha$ and $\beta$ are the variational parameters and are shown in Table 4, and $N_l(\zeta_k)$ is the normalization coefficient for the slater basis.

The total wave function $\Psi$ satisfies the Schrödinger equation $\mathrm{i}\frac{\partial}{\partial t}\Psi = H\Psi$, where $H = -\frac{1}{2}\nabla_r^2 + V_A + V_B$, $V_A/V_B$ are the interactions between the active electron and the projectile/target, respectively. After inserting the total wave function (4) into the above Schrödinger equation, the coupled equations for the amplitudes $A_j$ and $B_n$ (centered on the projectile and target, respectively) can be obtained as follows:

$$\mathrm{i}\left(\dot{A}_j + \sum_{m=N+1}^{N+M} S_{jm}\dot{B}_m\right) = \sum_{k=1}^{N} H_{jk}A_k + \sum_{m=N+1}^{N+M} K_{jm}B_m, \tag{7}$$

$$\mathrm{i}\left(\sum_{k=1}^{N} \bar{S}_{nk}\dot{A}_k + \dot{B}_n\right) = \sum_{k=1}^{N} \bar{K}_{nk}A_k + \sum_{m=N+1}^{N+M} \bar{H}_{nm}B_m, \tag{8}$$

where the dot denotes differentiation with respect to $t$, $S_{jm}$ is the overlap matrix, $H_{jk}$ and $H_{nm}$ are the direct matrices, and $K_{jm}$ and $K_{nk}$ are the exchange matrices.

The cross section $\sigma_{in}$ for electron capture can be obtained by solving the above coupled equation for the amplitudes under the initial condition $A_j(t \to \infty) = \delta_{ij}, B_n(t \to \infty) = 0$. If the incident channel is channel $i$, the probability for finding the system in the final state $n$ is

$$\sigma_{in} = 2\pi \int_0^{\infty} |B_n(t \to \infty)|^2 b\,\mathrm{d}b, \tag{9}$$

here $b$ is the impact parameter.

### 2.2. The model potentials

As mentioned in the preceding section, the interaction of the active electron with the target ion ($Li^+$) has been represented by a model potential as follows:

$$V_{\mathrm{Li}} = -\frac{1}{r} - \frac{2}{r}\mathrm{e}^{-3.31r} - 3.31\,\mathrm{e}^{-3.31r}. \tag{10}$$

In Table 1, we give the binding energies of the ground and excited states of $Li^{2+}$ ions and Li atoms which are obtained by the diagonalization of the single-electron Hamiltonian with the Coulomb and above model potentials. Moreover, the corresponding data from NIST are also given for comparison, good agreement with the calculated energies has been obtained.

**Table 1.** Energies (in units of a.u.) of $Li^{2+}$ ion and Li atom obtained by diagonalization of the single-electron Hamiltonian compared with the NIST data.

| | | $V_s$ (present) | NIST | Error |
|---|---|---|---|---|
| $Li^{2+}$ | 1s | –4.50000 | –4.50200 | 0.00044 |
| | 2s | –1.12500 | –1.12554 | 0.00048 |
| | 2p | –1.12500 | –1.12548 | 0.00043 |
| | 3s | –0.50000 | –0.50023 | 0.00045 |
| | 3p | –0.50000 | –0.50021 | 0.00042 |
| | 3d | –0.50000 | –0.50018 | 0.00037 |
| | 4s | –0.28122 | –0.28137 | 0.00054 |
| | 4p | –0.28125 | –0.28136 | 0.00041 |
| | 4d | –0.28125 | –0.28135 | 0.00037 |
| | 4f | –0.28125 | –0.28135 | 0.00035 |
| | 5s | –0.17972 | –0.18008 | 0.00197 |
| | 5p | –0.17999 | –0.18007 | 0.00045 |
| | 5d | –0.18000 | –0.18007 | 0.00037 |
| | 5f | –0.18000 | –0.18006 | 0.00035 |
| | 5g | –0.18000 | –0.18006 | 0.00035 |
| | 6s | –0.12380 | –0.12505 | 0.01000 |
| | 6p | –0.12493 | –0.12505 | 0.00095 |
| | 6d | –0.12498 | –0.12505 | 0.00052 |
| | 6f | –0.12500 | –0.12504 | 0.00035 |
| | 6g | –0.12500 | –0.12504 | 0.00035 |
| | 6h | –0.12500 | –0.12504 | 0.00034 |
| Li | $1s^2$2s | –0.19800 | –0.19822 | 0.00113 |
| | $1s^2$2p | –0.12994 | –0.13029 | 0.00268 |
| | $1s^2$3s | –0.07428 | –0.07421 | 0.00091 |
| | $1s^2$3p | –0.05720 | –0.05726 | 0.00104 |
| | $1s^2$3d | –0.05557 | –0.05563 | 0.00106 |
| | $1s^2$4s | –0.03867 | –0.03863 | 0.00100 |
| | $1s^2$4p | –0.03197 | –0.03199 | 0.00055 |
| | $1s^2$4d | –0.03126 | –0.03129 | 0.00085 |
| | $1s^2$4f | –0.03125 | –0.03126 | 0.00017 |

## 3. Results and discussion

### 3.1. Choice of the expansion basis

It is crucial to use a large expansion basis in the TC-AOCC method for ensuring the convergence of the cross section results. In Tables 2 and 3, we compare the $nl$-partial cross sections for the dominant ($n = 4$) and sub-dominant ($n = 3, 5, 6$) capture channels at the collision energies of 1 keV/u and 10 keV/u. For avoiding the problem of linear correlation of the expansion basis sets centered on the projectile and

target, different expansion basis sizes are used in the present calculation for different impact energy regions. In the energy range 0.1–2 keV/u, the projectile contains all bound states of $n \leq 8$ ($l \leq 5$), and the target contains all bound states of $n \leq 4$. For energies above 3 keV/u, the projectile contains all $n \leq 13$ ($l \leq 5$) bound states and 68 quasi-continuum pseudostates, while the target contains only all bound states of $n \leq 4$.

In Table 2, the cross sections calculated with different basis sets are compared for the impact energy of 1 keV/u. From this table, we can see that the *nl*-state-selective cross sections for the basis set $Li^{2+}(n \leq 8)/Li(n \leq 4)$ are very closed to those of basis set $Li^{2+}(n \leq 8)/Li(n \leq 5)$. It indicates that the basis placed on the target is reasonable. However, when compared with the results of basis set $Li^{2+}(n \leq 9)/Li(n \leq 2)$, we can see that there exist obvious differences in the *nl*-state-selective cross sections for both dominant and sub-dominant reaction channels. This means that the number of expansion basis set on the target is not enough. Further, by comparing the results of basis set $Li^{2+}(n \leq 8)/Li(n \leq 4)$ with those of basis set $Li^{2+}(n \leq 7)/Li(n \leq 4)$, it can be seen that the cross sections from these two basis sets are comparable. It means that the basis sets placed on the incident particles are reasonable.

In Table 3, the cross sections calculated with different basis sets are compared for the impact energies of 10 keV/u and 100 keV/u. The results are reliable for their convergence under the selected basis sets. A similar procedure is also performed below for the collision systems of $Li^{3+}$–$Li(1s^2 2p_0)$ and $Li^{3+}$–$Li(1s^2 2p_1)$.

**Table 2.** The *nl*-partial cross sections (in units of $10^{-16}$ cm$^2$) for the dominant and sub-dominant capture channels in $Li^{2+}$–$Li(1s^2 2s)$ collisions at 1 keV/u with different basis sets.

| *nl* | $Li^{2+}(n \leq 7)/Li(n \leq 4)$ | $Li^{2+}(n \leq 8)/Li(n \leq 4)$ | $Li^{2+}(n \leq 8)/Li(n \leq 5)$ | $Li^{2+}(n \leq 9)/Li(n \leq 2)$ |
|---|---|---|---|---|
| 3s | 0.74786 | 0.74525 | 0.74207 | 0.67981 |
| 3p | 2.78162 | 2.79866 | 2.79958 | 2.82756 |
| 3d | 1.26894 | 1.27982 | 1.28445 | 1.29247 |
| 4s | 12.78756 | 12.88953 | 12.87795 | 12.07162 |
| 4p | 32.57727 | 32.65314 | 32.72342 | 30.67455 |
| 4d | 49.70066 | 49.59046 | 49.60763 | 46.50709 |
| 4f | 82.62856 | 82.66100 | 82.64863 | 80.08355 |
| 5s | 0.72093 | 0.79581 | 0.82376 | 0.81078 |
| 5p | 2.29183 | 2.28852 | 2.23026 | 3.02780 |
| 5d | 3.95315 | 4.02875 | 4.13100 | 4.73969 |
| 5f | 3.90052 | 3.87196 | 3.91839 | 4.38944 |
| 5g | 1.65605 | 1.63617 | 1.61871 | 2.14910 |
| 6s | 0.23295 | 0.26380 | 0.25269 | 0.38003 |
| 6p | 0.90188 | 0.87596 | 0.90841 | 1.97223 |
| 6d | 1.02486 | 1.04176 | 0.97867 | 2.50951 |
| 6f | 0.87311 | 0.92330 | 0.91127 | 2.14721 |
| 6g | 0.79499 | 0.79785 | 0.78122 | 1.77867 |
| 6h | 0.34124 | 0.29657 | 0.32079 | 0.75191 |

**Table 3.** The *nl*-partial cross sections (in units of $10^{-16}$ cm$^2$) for the dominant and sub-dominant capture channels in $Li^{2+}$–$Li(1s^2 2s)$ collisions at energies of 10 keV/u and 100 keV/u with different basis sets.

| *nl* | $E = 10$ keV/u | | $E = 100$ keV/u | |
|---|---|---|---|---|
| | $Li^{2+}(n \leq 13)/Li(n \leq 4)$ | $Li^{2+}(n \leq 15)/Li(n \leq 6)$ | $Li^{2+}(n \leq 13)/Li(n \leq 4)$ | $Li^{2+}(n \leq 15)/Li(n \leq 6)$ |
| 3s | 0.64262 | 0.66742 | 0.00546 | 0.00435 |
| 3p | 2.87482 | 2.91122 | 0.05494 | 0.05645 |
| 3d | 5.69733 | 5.73932 | 0.04826 | 0.05352 |
| 4s | 0.85291 | 0.90728 | 0.00371 | 0.00294 |
| 4p | 4.16113 | 4.29256 | 0.02472 | 0.02627 |
| 4d | 12.82695 | 13.11016 | 0.02206 | 0.02246 |
| 4f | 50.18307 | 50.40761 | 0.00697 | 0.00880 |
| 5s | 0.74181 | 0.72777 | 0.00274 | 0.00193 |
| 5p | 2.66397 | 2.63733 | 0.01372 | 0.01439 |
| 5d | 7.31421 | 7.35082 | 0.01019 | 0.01065 |
| 5f | 14.34866 | 14.77341 | 0.00402 | 0.00556 |
| 5g | 14.44446 | 14.47175 | 0.00134 | 0.00150 |
| 6s | 0.52141 | 0.55310 | 0.00231 | 0.00130 |
| 6p | 1.73196 | 1.61667 | 0.00921 | 0.00993 |
| 6d | 4.03045 | 3.91881 | 0.00560 | 0.00540 |
| 6f | 5.16323 | 5.07694 | 0.00218 | 0.00288 |
| 6g | 3.72710 | 3.82662 | 0.00098 | 0.00117 |
| 6h | 1.65248 | 1.63444 | 0.00020 | 0.00021 |

**Table 4.** The variational parameters $\alpha$ and $\beta$ in the Slater basis for the projectile and target, respectively.

| | State | $\alpha$ | $\beta$ |
|---|---|---|---|
| $Li^{2+}$ | $n$s | 0.100 | 1.322 |
| | $n$p | 0.088 | 1.324 |
| | $n$d | 0.145 | 1.255 |
| | $n$f | 0.200 | 1.220 |
| | $n$g | 0.220 | 1.200 |
| | $n$h | 0.100 | 1.370 |
| Li | $n$s | 0.0805 | 1.334 |
| | $n$p | 0.090 | 1.334 |
| | $n$d | 0.085 | 1.355 |
| | $n$f | 0.100 | 1.370 |

### 3.2. $Li^{3+}$–Li($1s^2 2s$) collisions

The present total charge transfer cross sections for the collision of $Li^{3+}$–Li($1s^2 2s$) in the energy range 0.1–300 keV/u are shown in Fig. 1. In the same figure, the previous AOCC calculations by Schweinzer *et al.*[9] are also shown for comparison, and no other available data can be used for this collision system until now. It can be seen from this figure that the previous AOCC results of Schweinzer *et al.*[9] have the same energy-dependent behavior with our present results, but the magnitude of the previous AOCC cross section is obviously larger than the present result in the overlapping energy range. The difference between the results of different AOCC calculations maybe come from both the different model potentials used to represent the electron–ion interaction and the difference in the size of the AO expansion basis used in the dynamic calculations. It is noted that the present total charge exchange cross sections show a flat energy behavior for the collision energy below 10 keV/u. Above this energy, the present AOCC cross sections start to decrease sharply. The near flat energy behavior of the total charge exchange cross section in the energy region below 10 keV/u is a result of the different energy behavior of the $nl$-state-selective electron capture cross section in the same energy region.

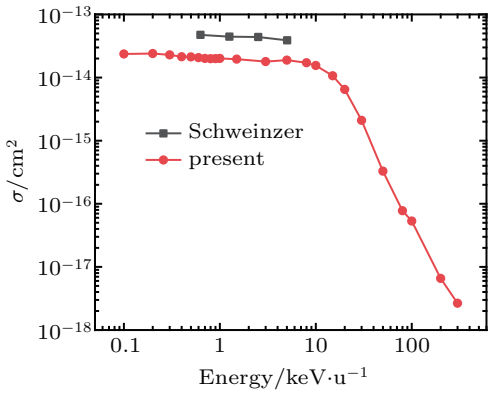



**Fig. 1.** Total charge exchange cross sections for $Li^{3+}$–Li($1s^2 2s$) collisions. Schweinzer refer to the results of Ref. [9].

Figure 2 shows our AOCC cross sections for electron capture to $n = 3$, 4, 5, 6, 7 shells of $Li^{2+}$ ion in the $Li^{3+}$–Li($1s^2 2s$) collisions. The theoretical CTMC results of Otranto *et al.*[10] in the same energy region are also shown for comparison. No other theoretical data have been reported for these $n$-partial cross sections. It can be observed that the electron capture to the $n = 4$ shell dominates in the energy region below $\sim$ 15 keV/u for this collision system, but for higher energies, the cross sections for capture to $n = 3$, 5, 6, 7 shells become comparable. In the overlapping energy region, the present AOCC results for capture to $n = 4$, 6, 7 shells of $Li^{2+}$ ion are in general agreement with the CTMC results of Otranto *et al.*[10] For the $n = 5$ shell, the present AOCC cross sections agree with the CTMC calculations by Otranto *et al.*[10] for the collision energies above 1.5 keV/u. While the present AOCC results for capture to the $n = 3$ shell agree poor with those of CTMC calculations[10] in the considered energy range. The significant disagreement between the present TC-AOCC results and CTMC calculations[10] in the low energy region can be attributed to a fact that CTMC is a full classical method and it is not suitable to describe the collision processes at the low collision energies. Furthermore, the CTMC method can not give the $n$- and $nl$-state-selective electron capture cross sections directly. Within that method, the determination of quantum numbers $(n, l, m)$ of the captured electron is based on the quantum–classical correspondence principle, which is appropriate only for high $n$ values. However, in the present TC-AOCC method, the use of suitable model potentials and very large expansion basis (including pseudostates) leads to an accurate description of the collision dynamics to generate convergent and accurate state-selective electron-capture cross sections in the intermediate collision energy region. It should be noted that all the $n$-partial electron capture cross sections (including the total charge transfer cross section in Fig. 1) decrease sharply for the collision energies above $\sim$10 keV/u. This decrease for the energy region above 10 keV/u is mainly due to a fact that the excitation and ionization processes become more important at the high collision energies.

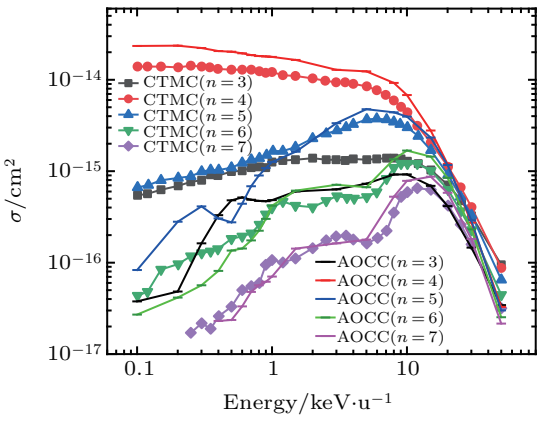



**Fig. 2.** Cross sections for electron capture to $n = 3$–7 shells of $Li^{2+}$ ion in $Li^{3+}$–Li($1s^2 2s$) collisions. CTMC data are from Ref. [10].

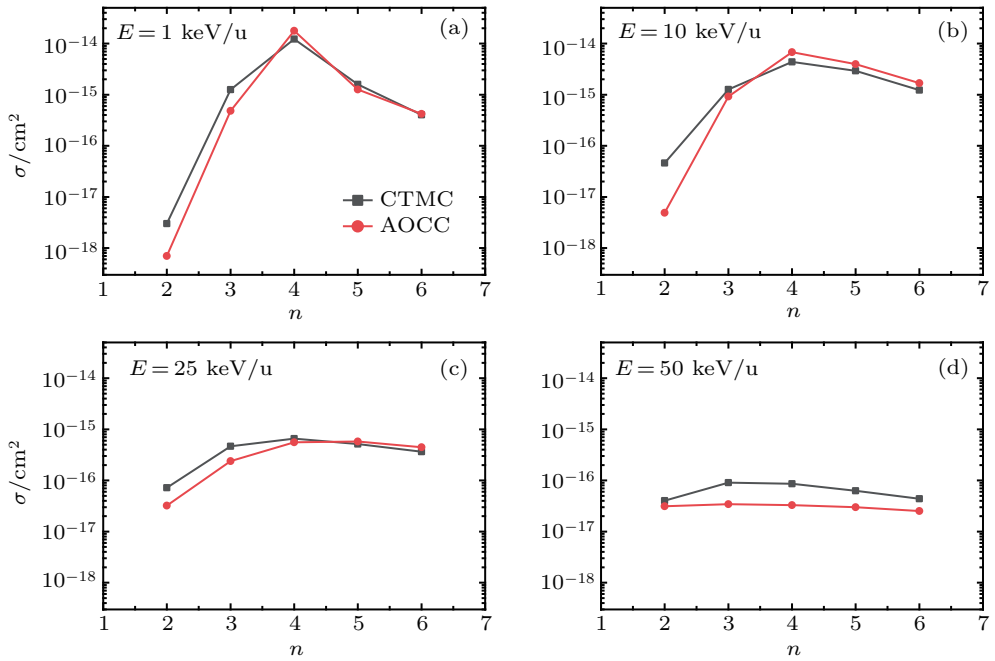



**Fig. 3.** The $n$-distributions of charge transfer cross sections for $Li^{3+}$–$Li(1s^22s)$ collisions at impact energies of (a) 1 keV/u, (b) 10 keV/u, (c) 25 keV/u, and (d) 50 keV/u.

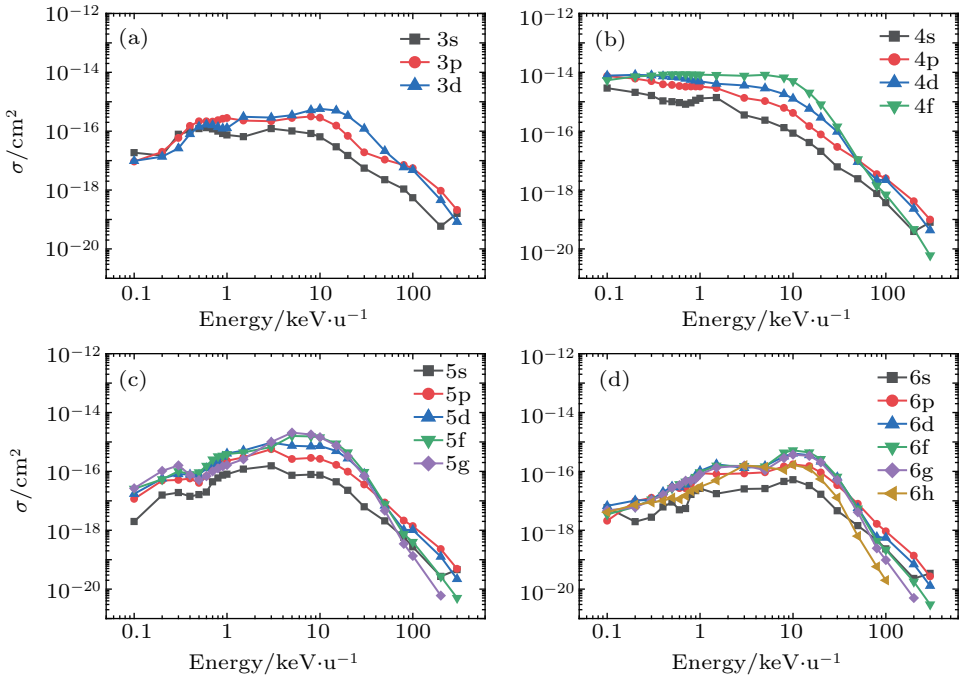



**Fig. 4.** Cross sections for electron capture to (a) $3l$, (b) $4l$, (c) $5l$, and (d) $6l$ states of $Li^{2+}$ ion as a function of the impact energy in $Li^{3+}$–$Li(1s^22s)$ collisions.

In Fig. 3, we show the $n$-distribution ($n$ = 2–6) of the charge transfer cross sections in $Li^{3+}$–$Li(1s^22s)$ collisions at impact energies of 1 keV/u, 10 keV/u, 25 keV/u, and 50 keV/u, respectively. The results of the present AOCC calculations are compared with the CTMC calculations of Otranto *et al.*[10] It can observed that for all considered impact energies, our $n$-distribution of the charge transfer cross sections is in general agreement with that of CTMC calculations,[10] especially for the low collision energies. It should be noted that for $E$ = 1 keV/u, the electron capture cross sections increase sharply with the increase of $n$, reach a maximum at $n = 4$, and then decrease sharply. This means that $n = 4$ is the dominant capture channel at this collision energy. We further note that with increasing collision energy, the charge transfer cross sections still first increase up to $n = 4$ and then decrease. But the magnitudes of the cross sections for capture to different $n$ shells become comparable, especially for the high energies. It is interesting to note that for $E$ = 50 keV/u, the charge transfer cross sections reach the maximum at $n = 3$, and then decrease slowly. It means that with increasing collision energy,

the captured electron will have a broad distribution on the different excited states of the projectile ions. It also demonstrates that only a large expansion basis can lead to the accurate $nl$-state-selective electron capture cross sections, especially for the high energies.

In Fig. 4, we present our AOCC state-selective cross sections for electron capture to the $3l$, $4l$, $5l$, and $6l$ states of $Li^{2+}$ ion in $Li^{3+}$–$Li(1s^22s)$ collisions, respectively. No other available data of state-selective cross sections has been reported for this collision system until now. It should be noted that for the weak electron capture channels ($3l$, $5l$, $6l$), there exist some oscillatory structures in the state-selective cross sections in the energy region below $\sim 1.5$ keV/u, these structures are from the more complex population dynamics at low collision energies for these $nl$ states.

### 3.3. $Li^{3+}$–$Li(1s^22p_{0,1})$ collisions

The total and partial cross sections for electron capture to $n = 3$–6 shells of $Li^{2+}$ ion in $Li^{3+}$–$Li(1s^22p)$ and $Li^{3+}$–$Li(1s^22p_1)$ collisions from the present AOCC calculations are displayed in Fig. 5. To the best of our knowledge, no other available data have been reported for these collision systems so far. From Fig. 5(a), we can see that for the $Li^{3+}$–$Li(1s^22p)$ system, the electron capture to the $n = 5$ shell dominates in the energy below 30 keV/u, but it coincides with the case of capture to the $n = 4$ shell for energies above 2 keV/u. In the energy region 3–5 keV/u, the magnitude of the $n = 6$ captured cross section becomes comparable with those of $n = 5$ and $n = 4$ shells. In the energy region above 50 keV/u, the $n = 3$ shell becomes the dominant reaction channel due to the momentum transfer. From Fig. 5(b), we can see that the electron capture to the $n = 5$ shell of $Li^{2+}$ ion dominates up to 5 keV/u. For the energy region 5–20 keV/u, the cross sections for electron capture to $n = 4$–6 shells become comparable. By comparing Fig. 5(a) with Fig. 5(b), it can be seen that the energy behavior and magnitude of the $n$-partial electron capture cross sections have significant difference for the collision energy below $\sim 20$ keV/u. This difference demonstrates that the $n$-partial electron capture cross sections are sensitive to the initial p-state charge cloud alignment, especially for the low collision energies. In the energy region above 20 keV/u, we can see that the magnitude and energy behavior of the $n$-partial cross sections from different initial target states are very similar.

Meanwhile, comparing Fig. 5 with the results from the initial $Li(1s^22s)$ state (shown in Fig. 2), we can see that the dominant electron capture channel and the magnitudes of the different $n$-partial electron capture cross sections all have significant changes for the case of $Li(1s^22p_{0,1})$ target.

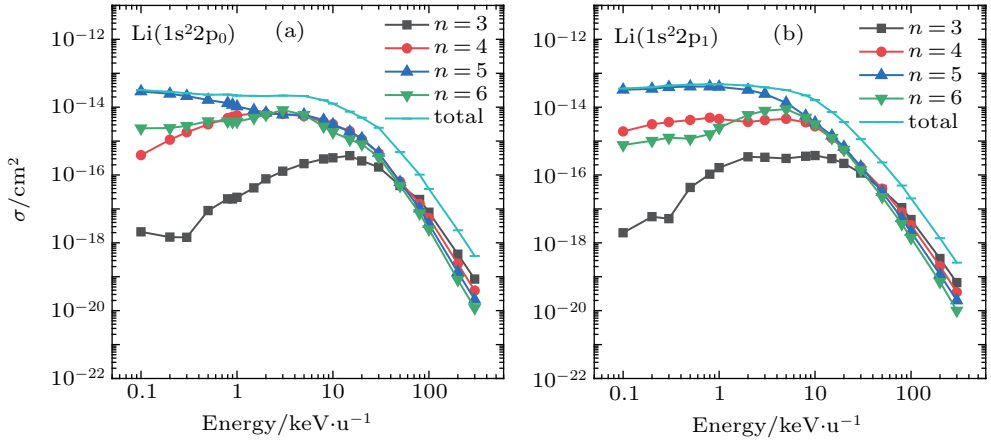



**Fig. 5.** Total and partial cross sections for electron capture to $n = 3$–6 shells of $Li^{2+}$ ion in (a) $Li^{3+}$–$Li(1s^22p_0)$ and (b) $Li^{3+}$–$Li(1s^22p_1)$ collisions.

The cross sections for charge transfer to the $3l, 4l, 5l$, and $6l$ states of $Li^{2+}$ ion in $Li^{3+}$–$Li(1s^22p_0)$ and $Li^{3+}$–$Li(1s^22p_1)$ collision systems are displayed in Figs. 6 and 7, respectively. No other theoretical or experimental data have been reported for these subshell-selective cross sections until now. It can be observed that for the dominant reaction channel, the magnitudes of the $5l$-capture cross sections are significantly larger than those of the subdominant channels in the energy region below about 1 keV/u for both collision systems. With increasing impact energy, for energies above 50 keV/u, the magnitudes of different subshell-selective cross sections become comparable. The more complex population dynamics of the $nl$ states at low energies result in some oscillatory energy behavior of the $nl$ cross sections in the low energy region. Comparing the partial charge exchange cross sections of the $Li^{3+}$–$Li(1s^22p_0)$ system with those of the $Li^{3+}$–$Li(1s^22p_1)$ system, we can see that there exist obviously differences in the magnitude and energy behavior of the $nl$-state-selective cross sections due to the strong alignment dependence on the initial targets.

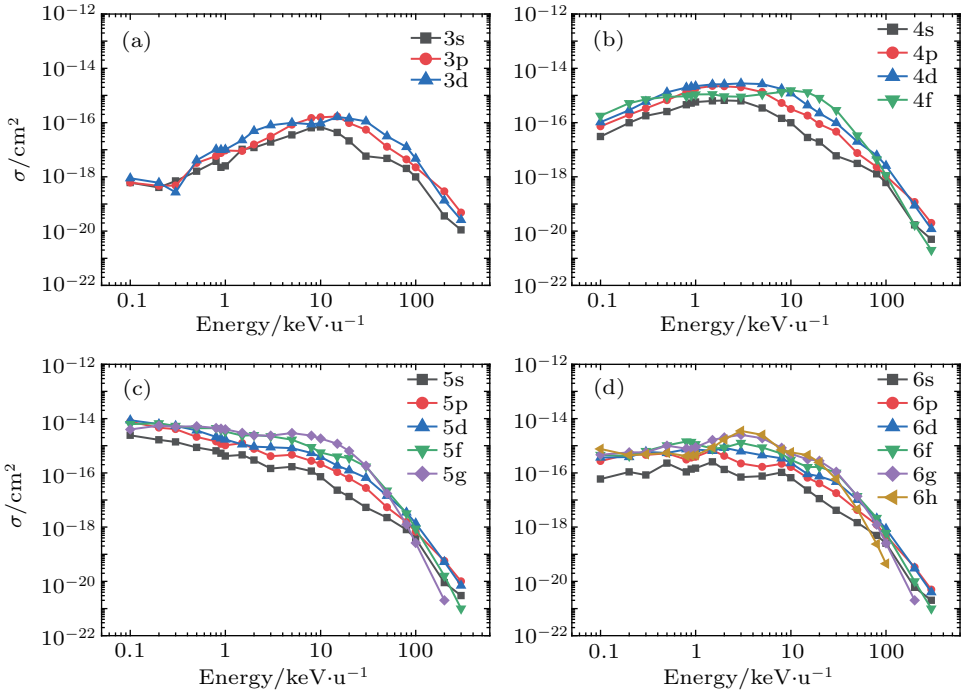



**Fig. 6.** State selective cross sections for electron capture to (a) 3*l*, (b) 4*l*, (c) 5*l*, and (d) 6*l* states of $Li^{2+}$ ion from the initial $Li(1s^22p_0)$ state.

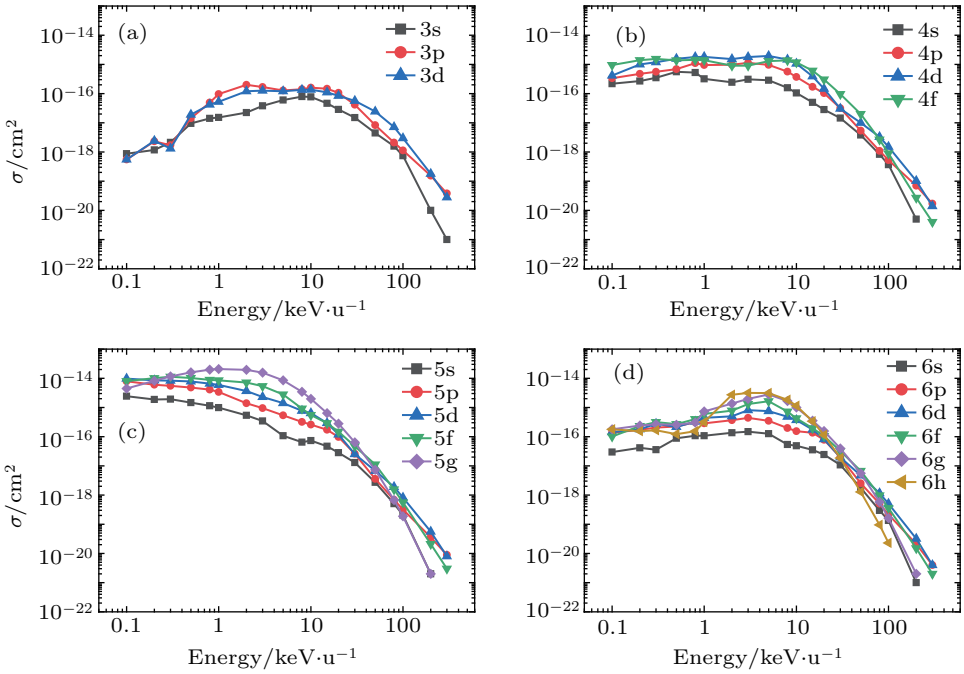



**Fig. 7.** State selective cross sections for electron capture to (a) 3*l*, (b) 4*l*, (c) 5*l*, and (d) 6*l* states of $Li^{2+}$ ion from the initial $Li(1s^22p_1)$ state.

In Fig. 8, we display the *n*-distribution of the charge exchange cross sections for the $Li^{3+}$–$Li(1s^22s)$ and $Li^{3+}$–$Li(1s^22p_{0,1})$ collision systems at impact energies of 1 keV/u, 10 keV/u, 50 keV/u, and 100 keV/u, respectively. It can be seen from this figure that for $E = 1$ keV/u, the dominant electron capture channel is the $n = 4$ shell for the $Li^{3+}$–$Li(1s^22s)$ system, while for the $Li^{3+}$–$Li(1s^22p_{0,1})$ collision systems, $n = 5$ is the dominant reaction channel. We further note that the magnitudes of the cross sections for these dominant reaction channels are significantly larger that those of the subdominant channels. With the increase of the collision energy, we can see that for $E = 50$ keV/u, the dominant electron capture channels for the $Li^{3+}$–$Li(1s^22s)$ and $Li^{3+}$–$Li(1s^22p_{0,1})$ systems become the $n = 3$ and $n = 4$ shells, respectively. For $E = 100$ keV/u, the dominant reaction channels for these three collision systems have all become the $n = 3$ shell, and the magnitudes of the cross sections for the dominant and subdominant channels become comparable.

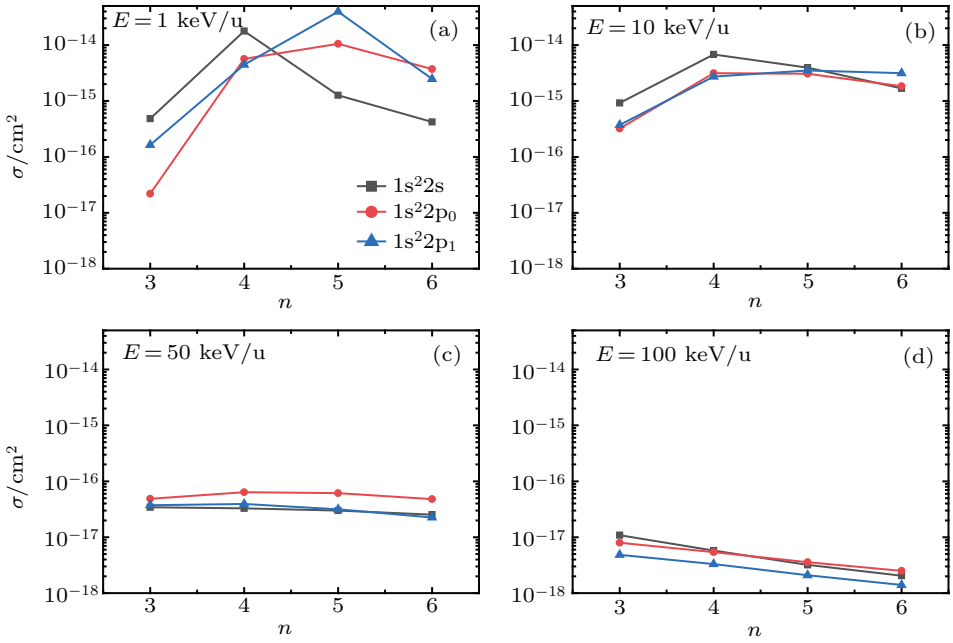



**Fig. 8.** The $n$ distributions of electron capture cross sections in $Li^{3+}$–$Li(1s^22s)$ and $Li^{3+}$–$Li(1s^22p_{0,1})$ collision systems at impact energies of (a) 1 keV/u, (b) 10 keV/u, (c) 25 keV/u, and (d) 50 keV/u.

## 4. Conclusion

In the present article, we have studied the charge exchange processes in the $Li^{3+}$–$Li(1s^22s)$ and $Li^{3+}$–$Li(1s^22p_{0,1})$ collision systems by using the two-center atomic orbital close-coupling method. The total and state-selective charge exchange cross sections for these collision systems are calculated in the energy region between 0.1 keV/u and 300 keV/u. The interaction of the active electron with the target ion is described by the one-particle model potential. The total and $n$-partial charge exchange cross sections for the $Li^{3+}$–$Li(1s^22s)$ system are in general agreement with the available theoretical data in the overlapping energy range. For the subshell-selective charge exchange cross sections, no other available data can be compared so far.

For the $Li^{3+}$–$Li(1s^22p_{0,1})$ collision systems, it is found that the energy behavior and magnitude of the total and partial charge exchange cross sections are significantly different in the energy region below about 20 keV/u due to the strong alignment dependence on the initial state at low energies. For energies above 20 keV/u, the magnitude and energy behavior of the $n$-partial cross sections from different initial target states are very similar. By comparing the results of the $Li^{3+}$–$Li(1s^22p_{0,1})$ collision systems with those of $Li^{3+}$–$Li(1s^22s)$ system, we note that except for the difference on the magnitude and energy behavior of the cross section, the dominant reaction channel has also changed from $n = 4$ for the $Li^{3+}$–$Li(1s^22s)$ system to $n = 5$ for the $Li^{3+}$–$Li(1s^22p_{0,1})$ systems in the low energy region.

## References


[1] Lisse C M, Dennerl K, Englhauser J, Harden M, Marshall F E, Mumma M J, Petre R, Pye J P, Ricketts M J, Schmitt J J and Trumper R G W 1996 *Science* **274** 205

[2] Lepp S, Stancil P C and Dalgarno A 2002 *J. Phys. B* **35** R57

[3] Isler R C 1994 *Plasma Phys. Control. Fusion* **36** 171

[4] Zakharov L E, Blanchard W, Kaita R, Kugel H, Majeski R and Timberlake J 2007 *J. Nucl. Mater.* **363–365** 453

[5] Schorn R P, Hintz E, Rusbuldt D, Aumayr F, Schneider M, Unterreiter E and Winter H 1991 *Appl. Phys. B* **52** 71

[6] Medley S S, Donń A J H, Kaita R, Kislyakov A I, Petrov M P and Roquemore A L 2008 *Rev. Sci. Instrum.* **79**

[7] Opradolcet J I C and R D P 1989 *J. Phys. B* **22** 1809

[8] Kumar A and Kimura M 1991 *Phys. Rev. A* **43** 217

[9] Schweinzer J D wutte H P W 1994 *J. Phys. B* **27** 137

[10] Otranto S, Hoekstra R and Olson R E 2014 *Phys. Rev. A* **89** 022705

[11] Bransden B H and McDowell M R C 1992 *Charge Exchange and the Theory of Ion-Atom Collisions* (1st Edn.) (New York: Clarendon Press) p. 39